

Kondo spectral functions at low-temperatures: A dynamical-exchange-correlation-field perspective.

Zhen Zhao^{1*}

1 Division of Mathematical Physics and ETSE, Lund University, PO Box 118, 221 00 Lund,
Sweden

* zhen.zhao@teorfys.lu.se

Abstract

We calculate the low-temperature spectral function of the symmetric single impurity Anderson model using a recently proposed dynamical exchange-correlation (xc) field formalism. The xc field, coupled to the one-particle Green's function, is obtained through analytic analysis and numerical extrapolation based on finite clusters. In the Kondo regime, the xc field is modeled by an ansatz that takes into account the different asymptotic behaviors in the small- and large-time regimes. The small-time xc field contributes to the Hubbard side-band, whereas the large-time to the Kondo resonance. We illustrate these features in terms of analytical and numerical calculations for small- and medium-size finite clusters, and in the thermodynamic limit. The results indicate that the xc field formalism provides a good trade-off between accuracy and complexity in solving impurity problems. Consequently, it can significantly reduce the complexity of the many-body problem faced by first-principles approaches to strongly correlated materials.

Copyright attribution to authors.

This work is a submission to SciPost Physics.

License information to appear upon publication.

Publication information to appear upon publication.

Received Date

Accepted Date

Published Date

1

2 Contents

3	1 Introduction	2
4	2 Theory	3
5	2.1 V _{xc} formalism for the SIAM	5
6	2.2 The SIAM V _{xc} at low-temperature	7
7	3 Results	7
8	3.1 Analytic insights from a dimer	7
9	3.2 Including hybridization with a finite cluster at zero- <i>T</i>	8
10	3.3 Ansatz of the symmetric SIAM V _{xc}	10
11	4 Conclusions and outlook	13
12	A Low temperature approximation of the V_{xc}	15
13	B Analytic V_{xc} of an impurity-free-electron dimer	16
14	C Calculating the Green's function at <i>T</i> = 0 using TDVP	18

15	D Solving the Green's function from the ansatz of the Vxc	18
16	References	19

17
18

19 1 Introduction

20 Quantum impurity models (QIMs), where one impurity with a small number of discrete levels
21 is coupled to a noninteracting bath with continuous degrees of freedom, have been extensively
22 studied during the past decades. Originally proposed to study the Kondo effect [1] where a
23 localized spin is screened by conducting electrons due to many-body correlations, QIMs remain
24 to this date the focus of vast interest for their applicability to different topical areas, such as
25 quantum transport through nanoscale devices [2–4], tunneling spectroscopy [5–7], magnetic
26 phase manipulation [8], and many-body entanglement [9, 10]. Moreover, the single-impurity
27 Anderson model (SIAM) [11], one of the basic QIMs variants, is used as an auxiliary system
28 for dynamical mean-field theory (DMFT) [12], a tool in first-principles studies of strongly
29 correlated systems in- and out-of equilibrium [13–15].

30 Because of this important usage, several types of quantum impurity solvers for the SIAM
31 have been developed. The thermodynamic properties of the SIAM can be exactly solved by
32 the numerical renormalization group (NRG) [16], the continuous-time quantum Monte Carlo
33 (QMC) algorithm [17] and Bethe-ansatz-based analytic approaches [18–20]. However, the
34 direct application of these solvers to the spectral properties of the SIAM is restricted by factors
35 such as the high computational cost of the original NRG, and the dynamical sign problem or
36 artifacts introduced by the analytic continuation in QMC. Hence advanced solvers arise with
37 sophisticated numerical methods, including generalized NRG [21–24], functional renormal-
38 ization group [25, 26], configuration interaction approximations [27], distributional exact di-
39 agonalization (ED) [28, 29], steady-state density functional theory (DFT) [30–32], expansion
40 QMC [33–35], and non-wave-function-based tensor network approaches [36, 37].

41 Nonetheless, in spite of these significant advances, there remains a demand for a theoretical
42 treatment of the SIAM which can i) capture spectral weights and energy scales of the Kondo
43 peak and the Hubbard bands in a conceptually and physically transparent way, and ii) be
44 computationally inexpensive in order to make those *ab initio* treatments that use the SIAM as
45 an auxiliary system more numerically affordable.

46 Recently, a Green's function-based dynamical exchange-correlation (xc) field formalism
47 [38] was proposed. Given the key quantity in the framework, the dynamical xc field (Vxc),
48 the single-particle Green's function, and thus the spectral function, can be solved by a direct in-
49 tegral in the time domain. The Vxc has been calculated exactly for one-dimensional (1D) finite
50 lattice models [39, 40] and within the random-phase approximation for the homogeneous elec-
51 tron gas [41]. For those systems, the temporal behavior of the Vxc, $V^{\text{xc}}(t) \sim V_0 + \sum_n A_n e^{-i\omega_n t}$,
52 can be seen as the sum of a constant term (complex for the homogeneous electron gas) plus
53 a small number of oscillating terms accounting for quasiparticle-like excitations. Accordingly,
54 the spectral weight is mainly distributed among a sharp peak (from the constant term V_0)
55 and continuous satellite bands that emerge from the oscillating terms in Vxc. Thus, a central
56 task in the approach is to determine the parameters defining Vxc, which naturally implies the
57 introduction of approximate estimates. For example, when applied to 1D half-filled Hubbard
58 lattice and spin- $\frac{1}{2}$ antiferromagnetic Heisenberg lattice at zero temperature, the formalism
59 approximates the exact lattice Vxc using finite clusters [39, 40]. Consequently, the spectral

60 functions are calculated with a good trade-off between accuracy and computational cost. The
 61 quasiparticle-like excitations in the Vxc and the favourable spectral results may be explained
 62 by a dynamical screening effect: at zero-temperature, exchange potential and many-body cor-
 63 relations together suppress many degrees of freedom and lead to only few (if not only one)
 64 dominant excitations ω_n .

65 In the local moment regime, some central features of the SIAM local spectral function have
 66 an immediate interpretation in terms of the Vxc language. Namely, the Hubbard band and the
 67 sharp Kondo resonance peak may be recognised as coming from a ‘constant’ term and several
 68 ‘quasiparticle-like’ excitation energies. However, the width of the Kondo peak, which is related
 69 to the Kondo temperature T_K , is exponentially small in the Coulomb interaction U , which is
 70 different from the Dirac- δ peak brought by a constant V_0 . Moreover, in the mixed valence
 71 regime, the lack of sharp peak seems to contrast with previous Vxc results from homogeneous
 72 lattice models [39, 40]. Therefore, in this paper, we perform a systematic study of the symmet-
 73 ric SIAM from the perspective of the Vxc formalism. Our purpose is two-fold: i) by studying
 74 the Vxc of a QIM at finite temperature (T), we examine how the low- T thermal excitation and
 75 the inhomogeneous setup of the system are reflected in Vxc; ii) we expect to shed new light
 76 on the SIAM by investigating the real-time response of the impurity, which is not always easily
 77 accessed in conventional self-energy-based approaches. By working directly in real time, it
 78 avoids the problem of analytic continuation associated with imaginary-time approaches.

79 This paper is organized as follows. In Sec. 2, we extend the Vxc formalism, originally
 80 proposed for zero-temperature (zero- T) systems [38], to finite-temperatures (finite- T). This
 81 is followed by an application of the developed description to the symmetric SIAM at half-filling,
 82 at temperatures upto around the Kondo temperature T_K , in Sec. 2.1. In Sec. 3, we first calculate
 83 the Vxc analitically on a dimer and numerically on a finite cluster. Based on that, we propose
 84 an ansatz for the SIAM Vxc, from which the local spectral function is obtained. Quantities such
 85 as the Kondo temperature and the height of the Kondo peak are re-interpreted within the Vxc
 86 framework. Finally, we provide our conclusive remarks and an outlook in Sec. 4.

87 2 Theory

88 We first derive the general finite- T Vxc formalism and then apply it to a discrete cluster at
 89 thermal equilibrium which represents an impurity coupled to a bath. The low- T Vxc is obtained
 90 by taking the limit $T \rightarrow 0$. We will use atomic units throughout this paper.

91 For a system with chemical potential μ at finite temperature $T = 1/\beta$, the generalized
 92 time-independent Hamiltonian is

$$\hat{K} = \hat{H} - \mu\hat{N}. \quad (1)$$

93 With $\mathbf{r} = (\mathbf{r}, \sigma)$ the space-spin variable, $\hat{\psi}(\mathbf{r})$ the field operator and $\hat{\rho}(\mathbf{r})$ the density operator,
 94 we have

$$\hat{H} = \int d\mathbf{r} \hat{\psi}^\dagger(\mathbf{r}) h_0(\mathbf{r}) \hat{\psi}(\mathbf{r}) + \frac{1}{2} \int d\mathbf{r} d\mathbf{r}' \hat{\psi}^\dagger(\mathbf{r}) \hat{\psi}^\dagger(\mathbf{r}') v(\mathbf{r}, \mathbf{r}') \hat{\psi}(\mathbf{r}') \hat{\psi}(\mathbf{r}), \quad (2)$$

95 where the single-particle term $h_0(\mathbf{r}) = -\frac{1}{2}\nabla^2 + V^{\text{ext}}(\mathbf{r})$ is a sum of kinetic energy and the ex-
 96 ternal field V^{ext} , $v(\mathbf{r}, \mathbf{r}') = \frac{1}{|\mathbf{r}-\mathbf{r}'|}$ is the Coulomb interaction, and the particle-number operator
 97 reads

$$\hat{N} = \int d\mathbf{r} \hat{\psi}^\dagger(\mathbf{r}) \hat{\psi}(\mathbf{r}) = \int d\mathbf{r} \hat{\rho}(\mathbf{r}) \quad (3)$$

98 The Vxc formalism is based on the finite- T time-ordered single-particle Green’s function
 99 [42]

$$i\bar{G}(\mathbf{r}t, \mathbf{r}'t') := \langle\langle \hat{\psi}(\mathbf{r}t); \hat{\psi}^\dagger(\mathbf{r}'t') \rangle\rangle = \text{Tr}\{\hat{\rho}_G \mathcal{T}[\hat{\psi}(\mathbf{r}t) \hat{\psi}^\dagger(\mathbf{r}'t')]\} \quad (4)$$

100 where \mathcal{T} is the real-time time-ordering symbol,

$$\hat{\rho}_G = Z_G^{-1} e^{-\beta \hat{K}} \quad (5)$$

101 is the statistical operator,

$$Z_G = \text{Tr}[e^{-\beta \hat{K}}] \quad (6)$$

102 is the grand canonical partition function, and

$$\hat{\psi}(rt) = e^{i\hat{K}t} \hat{\psi}(r) e^{-i\hat{K}t} \quad (7)$$

103 and its conjugate $\hat{\psi}^\dagger$ are the Heisenberg-picture field operators. The $\langle\langle \dots \rangle\rangle$ symbol denotes
104 the thermal ensemble average of the time-ordered operators. The equation of motion of the
105 Green's function in the Vxc scheme is

$$[i\partial_t - h(r)]\bar{G}(rt, r't') - V^{\text{xc}}(rt, r't')\bar{G}(rt, r't') = \delta(t-t')\delta(r-r'), \quad (8)$$

106 where $h(rt) = h_0(r) + V^{\text{H}}(r) - \mu$ contains the Hartree field $V^{\text{H}}(r) = \int dr' v(r, r') \text{Tr}\{\hat{\rho}_G \hat{\rho}(r')\}$.
107 The Vxc is defined to according to:

$$V^{\text{xc}}(rt, r't') i\bar{G}(rt, r't') := \int dr'' v(r, r'') \langle\langle \hat{\rho}(r''t) \hat{\psi}(rt); \hat{\psi}^\dagger(r't') \rangle\rangle - V^{\text{H}}(r) i\bar{G}(rt, r't'). \quad (9)$$

108 We note that for systems in equilibrium, the Vxc in the frequency domain and the self-energy
109 Σ , defined such that

$$\int dr'' dt'' \Sigma(rt, r''t'') \bar{G}(r''t'', r't') = V^{\text{xc}}(rt, r't') \bar{G}(rt, r't'), \quad (10)$$

110 are related by the following expression:

$$\frac{1}{2\pi} \int d\omega' V^{\text{xc}}(r, r'; \omega - \omega') \bar{G}(r, r'; \omega') = \int dr'' \Sigma(r, r''; \omega) \bar{G}(r'', r'; \omega). \quad (11)$$

111 A correlator g can be defined to factorize the high-order term $\langle\langle \hat{\rho}(r''t) \hat{\psi}(rt); \hat{\psi}^\dagger(r't') \rangle\rangle$
112 [38]:

$$\langle\langle \hat{\rho}(r''t) \hat{\psi}(rt); \hat{\psi}^\dagger(r't') \rangle\rangle = i\bar{G}(rt, r't') g(r, r', r''; t, t') \rho(r''), \quad (12)$$

113 where $\rho(r'') = \text{Tr}\{\hat{\rho}_G \hat{\rho}(r'')\}$ is the ensemble average of the electron density. We can define
114 a dynamical xc hole

$$\rho^{\text{xc}}(r, r', r''; t, t') = [g(r, r', r''; t, t') - 1] \rho(r''), \quad (13)$$

115 which fulfills a sum rule when the number of electrons is conserved (the derivation essentially
116 follows that of the zero- T case [38] except that ground-state expectation value is replaced by
117 thermal average)

$$\int dr'' \rho^{\text{xc}}(r, r', r''; t, t') = -\theta(t' - t), \quad (14)$$

118 where θ is the Heaviside step function. Substituting the higher-order term in Eq. (9) with the
119 xc hole, the xc potential can be written as

$$V^{\text{xc}}(rt, r't') = \int dr'' v(r, r'') \rho^{\text{xc}}(r, r', r''; t, t'), \quad (15)$$

120 which shows that the finite- T xc field can be interpreted as the Coulomb potential of a finite- T
121 xc hole. Furthermore, the xc hole fulfills an exact constraint

$$\rho^{\text{xc}}(\mathbf{r}, \mathbf{r}', \mathbf{r}'' = \mathbf{r}; t, t') = -\rho(\mathbf{r}), \quad (16)$$

122 which follows from the fact that the higher-order term $\langle\langle \hat{\rho}(\mathbf{r}''t)\hat{\psi}(\mathbf{r}t); \hat{\psi}^\dagger(\mathbf{r}'t') \rangle\rangle$, and thus
123 the correlator \mathbf{g} , vanishes at $\mathbf{r}'' = \mathbf{r}$, since $\hat{\rho}(\mathbf{r})\hat{\psi}(\mathbf{r}) = \hat{\psi}^\dagger(\mathbf{r})\hat{\psi}(\mathbf{r})\hat{\psi}(\mathbf{r}) = \mathbf{0}$. Here we may
124 see an advantage of the Vxc-Framework: the definition of finite- T Vxc introduced here is a
125 natural extension from the zero- T formalism, with ground state expectation values replaced
126 by thermal ensemble averages. The sum rule and the exact constraint which the xc hole fulfills
127 take the same form as the $T = \mathbf{0}$ case. Moreover, the time-dependence of the external field
128 can be included in a formally straightforward way ($\mathbf{h}(\mathbf{r}) \rightarrow \mathbf{h}(\mathbf{r}t)$ in Eq. (8), thus $V^{\text{H}}(\mathbf{r}t)$ and
129 $\rho(\mathbf{r}t)$ depends on time). In practice, however, Vxc can have a more complicated behavior
130 when the system is driven by a time-dependent potential from its ground state or thermal
131 equilibrium state. The low- T properties of the equilibrium SIAM Vxc is shown in the following
132 section.

133 2.1 Vxc formalism for the SIAM

134 The SIAM Hamiltonian reads

$$\hat{H}_{SIAM} = \epsilon_f(\hat{n}_{f\uparrow} + \hat{n}_{f\downarrow}) + U\hat{n}_{f\uparrow}\hat{n}_{f\downarrow} + \sum_{k\sigma} [\epsilon_k \hat{c}_{k\sigma}^\dagger \hat{c}_{k\sigma} + (\nu_k \hat{f}_\sigma^\dagger \hat{c}_{k\sigma} + \text{H.c.})]. \quad (17)$$

135 Here \hat{f}_σ^\dagger (\hat{f}_σ) creates (annihilates) an electron with spin σ on the impurity site, $\hat{n}_{f\sigma} = \hat{f}_\sigma^\dagger \hat{f}_\sigma$
136 is the corresponding number operator, $\hat{c}_{k\sigma}^\dagger$ ($\hat{c}_{k\sigma}$) creates (annihilates) a bath electron with
137 energy ϵ_k . Furthermore, ν_k is the hybridization amplitude, and ϵ_f and U are the impurity
138 on-site energy and Coulomb interaction, respectively. We consider a symmetric SIAM at half-
139 filling, which means

$$U + 2\epsilon_f = 0, \quad (18)$$

140 and the ensemble average

$$n_{f\sigma} = \text{Tr}\{\hat{\rho}_G \hat{n}_{f\sigma}\} = 0.5. \quad (19)$$

141 We also choose the number of fermionic sites (impurity + bath) L to be even. The local spectral
142 function can be obtained from the impurity Green's function, which can be written in the
143 Lehmann representation as

$$\begin{aligned} i\bar{G}_{ff,\sigma}(t, \beta) &= \langle\langle \hat{f}_\sigma(t); \hat{f}_\sigma^\dagger(0) \rangle\rangle \\ &= \theta(t) Z^{-1} \sum_{mn_+} e^{-\beta E_m} e^{-i(E_{n_+} - E_m)t} |\langle n_+ | \hat{f}_\sigma^\dagger | m \rangle|^2 \\ &\quad - \theta(-t) Z^{-1} \sum_{mn_-} e^{-\beta E_m} e^{i(E_{n_-} - E_m)t} |\langle n_- | \hat{f}_\sigma | m \rangle|^2, \end{aligned} \quad (20)$$

144 where we set $t' = \mathbf{0}$ since the system is in equilibrium, m, n_+ and n_- label eigenstates with
145 $L, L + 1$ and $L - 1$ electrons, respectively, and $Z = \sum_m e^{-\beta E_m}$ is the partition function. The
146 system has particle-hole symmetry, therefore we focus on the positive time, namely the particle
147 part,

$$i\bar{G}_{ff,\sigma}^P(t > 0, \beta) = Z^{-1} \sum_m e^{-\beta E_m} \sum_{n_+} a_{n_+,m;\sigma} e^{-i\omega_{n_+,m}t}, \quad (21)$$

148 where $\omega_{n_+,m} = E_{n_+} - E_m$ are the excitation energies and $\mathbf{a}_{n_+,m;\sigma} = |\langle n_+ | \hat{f}_\sigma^\dagger | m \rangle|^2$ their corre-
 149 sponding weight. The equation of motion of the Green's function reads

$$[i\partial_t - \epsilon_f - V^H - V_\sigma^{\text{xc}}(t, \beta)] \bar{G}_{ff,\sigma}(t, \beta) = \delta(t), \quad (22)$$

150 where the Hartree term $V^H = U n_{f\bar{\sigma}}$ is proportional to the density of impurity electron with
 151 opposite spin $\bar{\sigma} \neq \sigma$. Here, we emphasize that the V_{xc} is a result of the Coulomb inter-
 152 action and can be interpreted as the Coulomb potential of the xc hole, which can be seen
 153 from Eq. (15). However, for the SIAM, the hybridization between the impurity and the bath
 154 is also a crucial factor influencing the spectral properties. A dynamical hybridization field,
 155 also directly coupled to the Green's function in the equation of motion, can be defined within
 156 the V_{xc} -Framework. We incorporate the hybridization field into the V_{xc} so that the equation
 157 of motion has a simpler form, and with the given V_{xc} , the Green's function can be directly
 158 solved. To investigate the hybridization effect, we consider the noninteracting case ($U = \mathbf{0}$ in
 159 Eq. (17)). At zero- T , the impurity Green's function $\mathbf{G}_{ff,\sigma}$ can be analytically solved as

$$\mathbf{G}_{ff,\sigma}(\omega) = \frac{1}{\omega - \epsilon_f - \Delta(\omega)}, \quad (23)$$

160 where

$$\Delta(\omega) = \sum_k \frac{|v_k|^2}{\omega^+ - \epsilon_k} \quad (24)$$

161 is the hybridization function. $\Delta(\omega)$ can be calculated analytically by modeling the continuous
 162 bath as a tight-binding ring with N_c sites and hopping strength t_h , and the impurity site couples
 163 to one site with strength V (see Fig. 1). In this model, the SIAM parameters are given by
 164 $\epsilon_k = 2t_h \cos(k)$ and $v_k = \frac{V}{\sqrt{N_c}}$. When $|\epsilon_f|, V \ll 2|t_h|$, we approach the so-called wide-band
 165 limit (WBL), thus the hybridization function can be treated as a constant for $|\omega| \ll 2|t_h|$,

$$\Delta(\omega) = i\Gamma = i \frac{\pi V^2}{4t_h}. \quad (25)$$

166 Accordingly, we can solve the hybridization field:

$$V_{\text{nonint,WBL}}^{\text{xc}}(t) = i\Gamma\theta(-t). \quad (26)$$

167 The physical picture is as follows: the infinitely wide bath band leads to a broadening of
 168 the impurity level ϵ_f , which is represented by a purely imaginary hybridization field. This
 hybridization effect exists also for non-WBL or interacting cases.

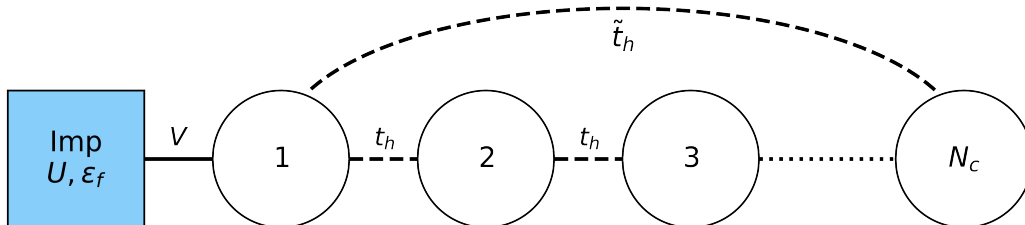


Figure 1: The 1D tight-binding system used to model an impurity coupled to a continuous bath. When periodic boundary conditions are used for the N_c noninteracting sites ($\tilde{t}_h = t_h$), we have the effective SIAM parameters $\epsilon_k = 2t_h \cos(k)$ and $v_k = \frac{V}{\sqrt{N_c}}$. When $\tilde{t}_h = 0$, the model approaches the SIAM setup in the large N_c limit.

170 2.2 The SIAM Vxc at low-temperature

171 The Vxc coupled to $\bar{\mathbf{G}}_{ff,\sigma}^P$ can be obtained from the equation of motion. For the symmetric
 172 SIAM at half-filling, $\epsilon_f + V^H = \mathbf{0}$, applying the Lehmann representation of $\bar{\mathbf{G}}_{ff,\sigma}^P$ (Eq. (21))
 173 into Eq. (22) and solving for the Vxc, we have

$$V_{p,\sigma}^{\text{xc}}(t, \beta) = \frac{\sum_m e^{-\beta E_m} \sum_{n_+} a_{n_+,m} \omega_{n_+,m} e^{-i\omega_{n_+,m} t}}{\sum_m e^{-\beta E_m} \sum_{n_+} a_{n_+,m} e^{-i\omega_{n_+,m} t}}. \quad (27)$$

174 We focus on the low-temperature case (referred to as low- T) such that $e^{-\beta E_m}$ is negligible
 175 except for the lowest two eigenstates $m = 1, 2$. Under this assumption, the Vxc can be written
 176 as (the derivation is in Appendix A)

$$V_{p,\sigma}^{\text{xc}}(t, \beta) = V_{p,\sigma}^{\text{xc}}(t, T = 0) + \tilde{V}_{p,\sigma}(t) e^{-\beta(E_2 - E_1)}, \quad (28)$$

177 which is the zero temperature $V_{p,\sigma}^{\text{xc}}(t, T = 0)$ plus a correction from a time-oscillating term
 178 $\tilde{V}_{p,\sigma}(t)$ and an exponentially small factor. Both the zero- T V^{xc} and the oscillating term \tilde{V} are
 179 determined by the interaction on the impurity site and the hybridization between the impurity
 180 and the bath. In the next section, we calculate analytically the low- T Vxc of a dimer where the
 181 interaction is nonzero on one site and present the Vxc of an SIAM on a finite cluster determined
 182 numerically. Our aim is to investigate the influence of the interaction U and the hybridization
 183 V on the Vxc, for the dimer and the cluster, respectively. We will then propose an ansatz for the
 184 finite- T SIAM Vxc and relate the ansatz parameters to the Kondo physics in the thermodynamic
 185 limit.

186 3 Results

187 3.1 Analytic insights from a dimer

188 We use a dimer with interaction U only on one site and hopping V between the sites to derive
 189 the analytic Vxc:

$$\hat{H}_{\text{dimer}} = \epsilon_f (\hat{n}_{f\uparrow} + \hat{n}_{f\downarrow}) + U \hat{n}_{f\uparrow} \hat{n}_{f\downarrow} + V \sum_{\sigma} (\hat{f}_{\sigma}^{\dagger} \hat{c}_{\sigma} + \text{H.c.}), \quad (29)$$

190 where we fix $\epsilon_f = -\frac{U}{2}$ and the dimer at half-filling. We consider the $T = 0$ case first. We study
 191 the large interaction regime ($U \gg V$) to obtain insights for the SIAM in the Kondo regime.
 192 The particle part of Vxc has an approximate form (for the derivation, see Appendix B)

$$V_{p,\sigma}^{\text{xc}}(t, T = 0) \approx \omega_p - \lambda \Omega e^{i\Omega t}, \quad (30)$$

193 where $\omega_p = \sqrt{\frac{U^2}{16} + 4V^2} + \sqrt{\frac{U^2}{16} + V^2}$, $\lambda \approx \frac{36V^2}{U^2}$, and $\Omega = \sqrt{\frac{U^2}{4} + 4V^2}$. Eq. (30) indicates that
 194 the dimer Vxc, similar to the cases mentioned in Sec. 1, can be seen as a sum of a constant term
 195 and a quasiparticle-like exponential term. Given the Vxc, the corresponding Green's function
 196 can be obtained by solving the equation of motion,

$$\begin{aligned} \bar{\mathbf{G}}_{ff,\sigma}^P(t, T = 0) &= \bar{\mathbf{G}}_{ff,\sigma}^P(0^+, T = 0) e^{-i(V^H + \omega_p)t} e^{i \int_0^t \lambda \Omega e^{i\Omega \bar{t}} d\bar{t}} \\ &\approx g^+ \left[(1 - \lambda) e^{-i(\epsilon_f + V^H + \omega_p)t} + \lambda e^{-i(\epsilon_f + V^H + \omega_0)t} \right], \end{aligned} \quad (31)$$

197 where $\omega_0 = \omega_p - \Omega \sim \frac{V^2}{U}$, $\mathbf{g}^+ = \bar{G}_{ff,\sigma}^p(\mathbf{0}^+, T = 0)$. For the symmetric model at half-filling,
 198 $\mathbf{g}^+ = -0.5\mathbf{i}$ and $\epsilon_f + V^H = 0$. The zero- T spectral function can be obtained with particle-hole
 199 symmetry,

$$A_{\text{dimer}}(\omega, T = 0) = \frac{1-\lambda}{2}\delta(\omega + \omega_p) + \frac{\lambda}{2}\delta(\omega + \omega_0) + \frac{\lambda}{2}\delta(\omega - \omega_0) + \frac{1-\lambda}{2}\delta(\omega - \omega_p). \quad (32)$$

200 Despite the obvious difference in complexity between the dimer and the SIAM, some physics
 201 of the SIAM can be outlined from the analytic expression of the dimer Vxc: for large U , two
 202 peaks ($\omega = \pm\omega_p$) of the spectral function are present, which correspond to impurity levels
 203 $\epsilon_f, \epsilon_f + U$. The excitation with energy Ω creates two central peaks at $\omega = \pm\omega_0 \approx 0$. However,
 204 for the dimer the spectral weights of the central peaks, $\frac{\lambda}{2} \sim (\frac{V}{U})^2$, vanish as U increase. The
 205 lack of Kondo resonance can be naturally understood as the impurity site is coupled to a single
 206 site instead of a continuous bath. This is directly reflected by the Vxc: as U increases, the
 207 exponential term (with amplitude $\lambda\Omega \sim \frac{V^2}{U}$) becomes negligible.

208 For low- T , the time-oscillating term in Eq. (28) can be written as

$$\frac{\tilde{V}_{p,\sigma}(t)}{V_{p,\sigma}^{\text{xc}}(t, T = 0)} \approx \lambda' e^{i\Omega' t} - \lambda'' e^{i\Omega'' t}, \quad (33)$$

209 where $\lambda', \lambda'' \sim \frac{V^2}{U^2}$, $\Omega' \sim U$ and $\Omega'' \sim \frac{V^2}{U}$ (see full expressions in Eqs. (B.27),(B.28), and
 210 (B.29) in Appendix B). The Vxc is then

$$V_{p,\sigma}^{\text{xc}}(t, \beta) \approx \omega_p - \lambda\Omega e^{i\Omega t} + e^{-\beta\Delta_0} \omega_p (\lambda' e^{i\Omega' t} - \lambda'' e^{i\Omega'' t}), \quad (34)$$

211 where $\Delta_0 \sim \frac{V^2}{U}$. Note that we require low temperature condition $e^{-\beta\Delta_0} \ll 1$. The particle
 212 spectral function is

$$A_{\text{dimer}}(\omega > 0, \beta) \cong \frac{1-\lambda - e^{-\beta\Delta_0} \omega_p (\frac{\lambda''}{\Omega''} - \frac{\lambda'}{\Omega'})}{2} \delta(\omega - \omega_p) + \frac{\lambda}{2} \delta(\omega - \omega_0) \\ + \frac{e^{-\beta\Delta_0} \omega_p \frac{\lambda''}{\Omega''}}{2} \delta(\omega - \tilde{\omega}_p) - \frac{e^{-\beta\Delta_0} \omega_p \frac{\lambda'}{\Omega'}}{2} \delta(\omega - \tilde{\omega}_0), \quad (35)$$

213 where $\tilde{\omega}_0 = \omega_p - \Omega'$ and $\tilde{\omega}_p = \omega_p - \Omega''$. The first two terms on the RHS of Eq. (35) corre-
 214 spond to the original peaks at zero- T , while the last two terms, with weights proportional to
 215 $e^{-\beta\Delta_0}$, represent two small peaks (referred to as thermal peaks in the text below) close to the
 216 original zero- T peaks, respectively. These thermal peaks arise from expanding the Lehmann
 217 representation of the Green's function to the order $e^{-\beta\Delta_0}$. Effectively, the peak at finite- T can
 218 be seen as the original peak at zero- T absorbing a thermal peak with close frequencies. Thus
 219 the temperature-induced broadening of the SIAM spectral peaks may be explained in the Vxc
 220 picture: *at low- T , thermal fluctuations induce new peaks close to the original peaks*. The energy
 221 difference between the original peak and the thermal peak gives effectively the width of the
 222 finite- T spectral peak.

223 3.2 Including hybridization with a finite cluster at zero- T

224 To investigate the combined effects of the interaction U and the hybridization V , we numeri-
 225 cally solve the Vxc for a finite cluster (corresponding to the $\tilde{\mathbf{t}}_h = \mathbf{0}$ case in Fig. 1)

$$\hat{H}_{\text{cluster}} = \epsilon_f(\hat{n}_{f\uparrow} + \hat{n}_{f\downarrow}) + U\hat{n}_{f\uparrow}\hat{n}_{f\downarrow} + V \sum_{\sigma} (\hat{f}_{\sigma}^{\dagger} \hat{c}_{1\sigma} + \text{H.c.}) + \sum_{i,\sigma}^{N_c-1} (t_h \hat{c}_{i,\sigma}^{\dagger} \hat{c}_{i+1,\sigma} + \text{H.c.}), \quad (36)$$

226 where N_c is the number of noninteracting sites. In the limit $N_c \rightarrow \infty$, we reproduce the
 227 continuous bath (equivalent to $\epsilon_k = 2t_h \cos(k)$, $v_k = \frac{V}{\sqrt{N_c}}$ in Eq. (17)). We use the ITensor
 228 library [43,44] to perform the time-dependent variational principle (TDVP) [45,46] algorithm
 229 on a symmetric cluster with $L = N_c + 1 = 50$ sites at zero- T (the algorithm performs better
 230 in system with open boundary conditions, hence we use a chain setup instead of a periodic
 231 one. See detailed treatment in Appendix C). We show in Fig. 2 $\text{Re}V^{\text{xc}}(t)$ with different V
 232 values. Also, we plot $\text{Re}V^{\text{xc}}(\omega)$ to analyze the excitation terms contained in the Vxc. For fixed
 233 model parameters $\epsilon_f = -2.5$, $U = 5$, $t_h = -1$, $\text{Re}V^{\text{xc}}(t)$ with different V can be seen to have
 234 three main features. i) It oscillates around some constant values close to $\frac{U+V}{2}$. The constant
 235 terms increase with V and correspond to the sharp peaks of $\text{Re}V^{\text{xc}}(\omega)$ at $\omega = 0$. ii) The local
 236 maxima of $\text{Re}V^{\text{xc}}(t)$ are approximately equally separated (e.g. for $V = 1$, the time intervals
 237 between local maximums are almost 1.85), which may be described by a factor $\mathcal{A}e^{-i\omega_p t}$. The
 238 excitation energy ω_p corresponds to the peaks of $\text{Re}V^{\text{xc}}(\omega)$ at $\omega \sim -3$. Both the amplitude \mathcal{A}
 239 and the energy $|\omega_p|$ decrease as V turns smaller, as shown in the inset of Fig. 2 (right panel).
 240 iii) For $V = 1$, the local maximum of $\text{Re}V^{\text{xc}}(t)$ around $t = 1$ is much larger than other local
 241 maximal values. Correspondingly, $\text{Re}V^{\text{xc}}(\omega)$ exhibits non-Lorentzian structures for $\omega < -5$.
 242 Similar larger local maximum at small time also exists for $V = 0.5, 0.2$. As shown in the inset
 243 of Fig. 2 (left panel), for $V = 0.5$, the local maximum at $t \sim 2$ is nearly twice as large as
 244 the local maximum at $t \sim 4$. This drop in local maxima suggests that ω_p may contain an
 245 imaginary part.

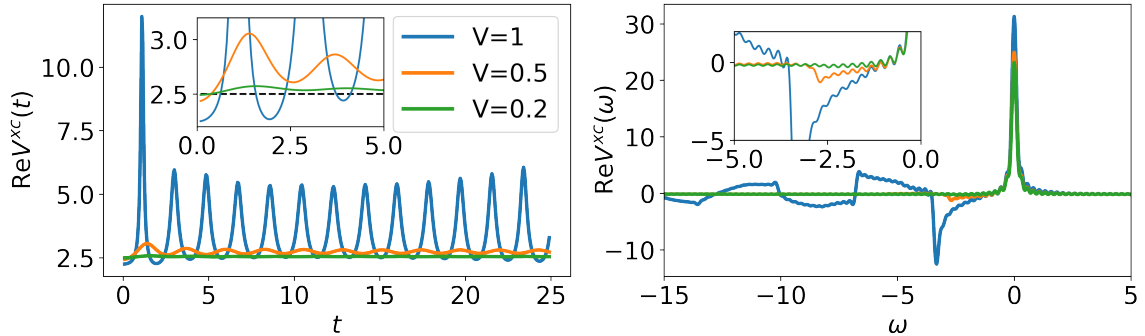


Figure 2: The Vxc of a 50-site cluster at half-filling, with parameters $\epsilon_f = -2.5$, $U = 5$, $t_h = -1$, $T = 0$. Left: real part of $V^{\text{xc}}(t)$. Right: real part of $V^{\text{xc}}(\omega)$, calculated with broadening factor $\eta = 0.1$.

246 Features i) and ii) can be already found in the analytic expression of the dimer Vxc. How-
 247 ever, feature iii) emerges only when the impurity is coupled to a large number of noninteracting
 248 sites. Therefore, we attribute feature iii) to the hybridization effect. As mentioned in Sec. 2.1,
 249 the Vxc here incorporates the hybridization field, which is a purely imaginary constant for the
 250 noninteracting case in the WBL. We note that the constant term of the cluster Vxc has a very
 251 small imaginary part. As a result, the spectral function exhibits sharp peaks at $\omega \sim \frac{U}{2}$, instead
 252 of proper Hubbard side-bands. This can be attributed to the qualitative difference between
 253 the Anderson-type chain with 50 sites and the SIAM where the bath has continuous degrees
 254 of freedom.

255 To summarize the finite-cluster results, $\text{Re}V^{\text{xc}}(t)$ exhibits an oscillating behavior, which
 256 suggests that the Vxc can still take the form $V^{\text{xc}}(t) = \mathcal{A}e^{-i\omega_p t} + \mathcal{C}$. However, the hybridization
 257 between the impurity and the bath requires a complex \mathcal{C} , so that $\text{Re}\mathcal{C}$ and $\text{Im}\mathcal{C}$ determine the
 258 peak location and the width of the Hubbard band, respectively. Moreover, the local maxima
 259 of $\text{Re}V^{\text{xc}}(t)$ change in time, suggesting a complex ω_p . Here, we notice that $\text{Im}[\omega_p]$ can be
 260 positive, leading to $V^{\text{xc}}(t) \rightarrow \infty$ for large positive t . Thus it is more appropriate to use the

261 form $V^{\text{xc}}(\mathbf{t}) = Ae^{-i\omega_p t} + C$, which is derived using finite clusters, in the small-time regime.

262 To determine the Vxc in the large-time regime ($|t_l| \rightarrow \infty$), we consider the following ob-
 263 servation. The spectral function at low energies is largely determined by $\bar{G}_{ff,\sigma}(t_l, \beta)$. The
 264 Kondo resonance peak (with half-width Γ_K) in the spectral function suggests that the Green's
 265 function in the large-time regime takes the form $\bar{G}_{ff,\sigma}(t_l > 0, \beta) \propto e^{-\Gamma_K t_l}$. Since in our
 266 formalism $\bar{G}_{ff,\sigma}(t > 0, \beta) \propto e^{-i \int_0^t V^{\text{xc}}(\bar{t}) d\bar{t}}$, the Vxc in the large-time regime should be ap-
 267 proximately $V^{\text{xc}}(t_l > 0) \approx -i\Gamma_K$. Notably, the fact that V^{xc} converges to $-i\Gamma_K$ for large positive
 268 t is a direct consequence of the Kondo effect. V^{xc} calculated using small finite clusters lacks
 269 this feature because the noninteracting bath is not continuous.

270 3.3 Ansatz of the symmetric SIAM Vxc

271 Based on the analytic and numerical results above, the particle part of $V^{\text{xc}}(t > 0)$ of the
 272 symmetric SIAM at low- T in the small- and large-time regimes can be described as:

$$V_{p,\sigma}^{\text{xc}}(t > 0, \beta) \approx \begin{cases} \lambda\omega_p e^{-i\omega_p t} + C, & t \text{ small} \\ -i\Gamma_K, & t \text{ large.} \end{cases} \quad (37)$$

273 The physical picture is highlighted as follows: V^{xc} in the large-time regime, dominating $\bar{G}_{ff,\sigma}$
 274 for large $|t|$, leads to the sharp Kondo resonance peak. On the other hand, V^{xc} in the small-
 275 time regime, with a large contribution from the constant term C , corresponds to the Hubbard
 276 side-band broadened by the hybridization effect. We propose an ansatz for $V_{p,\sigma}^{\text{xc}}(t > 0, \beta)$
 277 which captures both the large- and small-time features:

$$V_{p,\sigma}^{\text{xc}}(t > 0, \beta) = \frac{\lambda(\omega_p + C) + (1 - \lambda)Ce^{i\omega_p t}}{\lambda + (1 - \lambda)e^{i\omega_p t}}, \quad (38)$$

278 where λ is real, ω_p and C are complex, and $\omega_p + C = -i\Gamma_K$ is temperature-dependent. The
 279 fractional form of the complete ansatz (Eq. (38)) follows naturally from a Vxc obtained via the
 280 equation of motion and the Lehmann representation of the Green's function (see Eq. (27)),
 281 where both the numerator and the denominator contain exponential factors of t . Note that
 282 for a particle-hole symmetric system, the hole part Vxc ($t < 0$) can be calculated using the
 283 symmetry relation

$$V^{\text{xc}}(-t) = -V^{\text{xc}}(t). \quad (39)$$

284 Following Eq. (38), the local Green's function ($t > 0$) is then (see the derivation in Appendix D)

$$\bar{G}_{ff,\sigma}^p(t, \beta) = -\frac{i}{2} \left[(1 - \lambda)e^{-iCt} + \lambda e^{-i(C + \omega_p)t} \right], \quad (40)$$

285 and the spectral function is

$$A(\omega > 0, \beta) = \frac{1 - \lambda}{2\pi} \frac{|\text{Im}[C]|}{(\omega - \text{Re}[C])^2 + (\text{Im}[C])^2} + \frac{\lambda}{2\pi} \frac{|\text{Im}[C + \omega_p]|}{(\omega - \text{Re}[C + \omega_p])^2 + (\text{Im}[C + \omega_p])^2}, \quad (41)$$

286 and A for $\omega < 0$ can be calculated using the particle-hole symmetry:

$$A(\omega < 0, \beta) = A(-\omega, \beta). \quad (42)$$

287 Before determining the ansatz parameters numerically, we use the ansatz to interpret the
 288 Kondo spectral function. The two peaks in the spectral function can be recognized as a Hub-
 289 bard side-band located at $\omega = \text{Re}[C]$ with half-width $\Gamma_H = -\text{Im}[C]$, and a Kondo peak located

290 at $\omega = \text{Re}[C + \omega_p] = \mathbf{0}$ with half-width $\Gamma_K = -\text{Im}[C + \omega_p]$. The spectral weights of the two
 291 peaks are determined by λ . The two peaks have distinct origins. The peak location and the
 292 width of the Hubbard side-band are controlled by the constant term of the Vxc in the small-
 293 time regime, which accounts for the fact that the impurity level is affected by the interaction
 294 and broadened by the continuous bath. On the other hand, at low- T , the Vxc in the large-
 295 time regime creates a sharp resonance peak close to $\omega = \mathbf{0}$, whose width and height can be
 296 described by the Fermi-liquid treatment [47].

297 Having in mind the physical meaning of the parameters, we discuss the extrapolation proce-
 298 dure, i.e., how the ansatz quantities (λ, ω_p, C) can be calculated with a given symmetric
 299 SIAM with model parameters (U, V, t_h, β) . Here, to compare with NRG results in the litera-
 300 ture (e.g., from Refs. [29] and [48]), we also use the WBL. We consider first the $T = \mathbf{0}$ limit,
 301 and assume that the half-width of the Kondo peak is given by the Kondo temperature (T_K) [48].
 302 Thus,

$$C + \omega_p \Big|_{T=0} \approx -iT_K = -i \sqrt{\frac{U\Gamma}{2}} e^{-\frac{\pi U}{8\Gamma} + \frac{\pi i}{2U}}. \quad (43)$$

303 The peak location of the Hubbard side-band can be directly calculated, which means

$$\text{Re}[C] \approx \frac{U}{2}. \quad (44)$$

304 We notice that the height of the Kondo peak at $T = \mathbf{0}$ is given by $1/(\pi\Gamma)$, suggesting

$$A(\omega = \mathbf{0}) = \frac{\lambda}{\pi T_K} + \frac{1 - \lambda}{\pi |\text{Im}[C]|} = \frac{1}{\pi\Gamma}, \quad (45)$$

305 which simplifies to $\frac{\lambda}{\pi T_K} = \frac{1}{\pi\Gamma}$ for T_K much smaller than the Hubbard side-band half-width
 306 Γ_H , and thus λ can be determined. The last unknown parameter is the imaginary part of
 307 C , which corresponds to Γ_H . We use the Anderson-type finite-size chain spectral function to
 308 estimate $\text{Im}[C]$. Note that a finite chain cannot reproduce the proper broadening caused by an
 309 infinitely wide band. However, the relative weight between the Hubbard peak and the Kondo
 310 peak,

$$R = \frac{1 - \lambda}{2\lambda} \frac{T_K}{|\text{Im}[C]|}, \quad (46)$$

311 can provide information of $\text{Im}[C]$. We extrapolate the value of R by increasing the number of
 312 sites in the chain. We calculate the spectral function using the chain setup with an increas-
 313 ing number of noninteracting sites N_c . From the spectral functions (as plotted in Fig. 3a),
 314 we determine the relative weight R , which is then plotted against the total number of sites
 315 $L = N_c + 1$. For a given Γ , R increases with L (we use $L = 4, 8, 20, 30$ and 40), as shown by
 316 the scattered data points in Fig. 3b. Noticing the nearly linear increase of R at small L and
 317 expecting a converging R at large L , we fit the $R - L$ data using a hyperbolic-tangent func-
 318 tional form (which eventually provides satisfactory spectral functions) for the fitting function.
 319 Consequently, $R(L = \infty)$ can be estimated using the fitting results (see the curves in Fig. 3b).

320 In Fig. 4, we show the local spectral function of a symmetric SIAM in the WBL with
 321 $U = 3, t_h = 50, T = \mathbf{0}$. We choose the parameters ($\Gamma = 0.2, 0.5$, and 0.9) to compare with
 322 NRG results [29] in the WBL. The spectral function show satisfactory agreements to the NRG
 323 results. We attribute this to the fact that the Vxc as an effective field captures the intrinsic
 324 physics of an impurity problem. In the large-positive-time regime, $V_{p,\sigma}^{\text{xc}}(\mathbf{t})$ converges to
 325 $\omega_p + C = -iT_K$, meaning that the Kondo resonance peak is created at $\omega = \mathbf{0}$ and it requires
 326 no energy transfer. In the small-positive-time regime, $V_{p,\sigma}^{\text{xc}}(\mathbf{t})$ is dominated by the complex
 327 constant C , giving rise to the Hubbard side-band. Upon closely comparing our results with
 328 NRG, we notice that in the Kondo regime (small Γ/U), our Kondo peaks have a smaller width

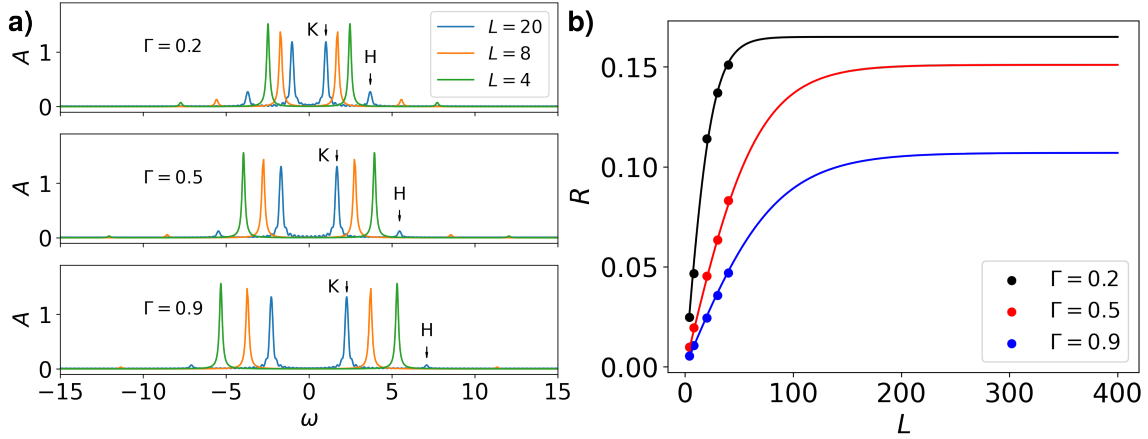


Figure 3: **a)** The zero- T spectral function of L -site clusters. We use $U = 3$, $t_h = 50$ to approach the WBL, and different V values to reach $\Gamma = 0.2, 0.5$ and 0.9 . The results are from ED for $L = 4, 8$ and from TDVP for $L = 20$. The Kondo peaks and Hubbard peaks are highlighted by arrows. **b)** The relative weight R between the Hubbard peak and the Kondo peak, as a function of the total number of sites L . TDVP is used for $L = 20, 30$ and 40 . For each value of Γ , the data are fitted using $R = R_\infty \tanh(aL)$, where R_∞ is the converged value and a is a parameter determining the converging speed. The fitted values are $R_\infty = 0.165, 0.151$, and 0.107 for $\Gamma = 0.2, 0.5$, and 0.9 , respectively.

329 than those from NRG. This is because we assume $\Gamma_K|_{T=0} = T_K$, while in NRG-based theory,
 330 $\Gamma_K|_{T=0} = w T_K$, where $w \approx 3.7$ is determined by the so-called Wilson number [49]. At zero- T
 331 and in the WBL, most of the ansatz parameters can naturally be determined based on some
 332 well-known results of the SIAM. Only one parameter requires a numerical extrapolation. More-
 333 over, the cluster spectral function used in the extrapolation (obtained via ED or TDVP) is actu-
 334 ally distinct from the SIAM spectral function: for cluster results, the Kondo peak position is
 335 not at $\omega = 0$, and the Hubbard band is too sharp. As already noted close to the end of section
 336 3.2, the discrepancy can be attributed to the essential differences between a finite cluster with
 337 tens of sites and a continuous bath. However, the Vxc scheme produces favourable spectral
 338 functions using these finite cluster results. This indicates that the Vxc formalism, originat-
 339 ing from very fundamental physics and using established knowledge of the target system as a
 340 reference, is able to capture the key features of the impurity problem.

341 Lastly, we discuss the spectral function at finite temperatures. In the Vxc formalism, we
 342 can see from the dimer result that thermal excitation leads to the broadening of both the
 343 Kondo peak and the Hubbard side-band peak. For the SIAM in the WBL, as the temperature
 344 T increases, the Kondo peak is broadened, while the Hubbard side-band remains almost un-
 345 changed. This thermal behavior can be effectively captured by our ansatz, which treats the
 346 imaginary part of the excitation energy ω_p as temperature-dependent, while assuming that
 347 other parameters remain temperature-independent. The temperature dependence can be ex-
 348 pressed as

$$\omega_p(T) = \omega_p(T=0) + i\Omega_T. \quad (47)$$

349 According to our interpretation of the ansatz parameters, ω_p at finite- T corresponds to the
 350 finite- T Kondo peak half-width Γ_K as

$$\omega_p(T) = -\frac{U}{2} + i[\Gamma_H - \Gamma_K(T)]. \quad (48)$$

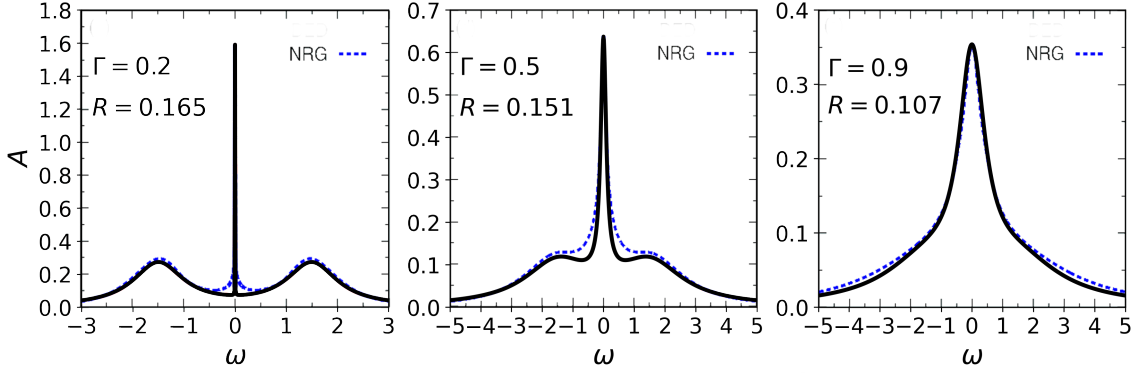


Figure 4: The zero- T spectral function of a symmetric SIAM. We use $U = 3$, $t_h = 50$ to approach the WBL, and different V values to realize desired Γ values. From the extrapolation, we get $\text{Im}[C] = -0.6, -1.3$ and -1.7 , respectively, for $\Gamma = 0.2, 0.5$ and 0.9 . The NRG results (blue dashed lines) are adapted from Ref. [29].

351 Following Eqs. (47) and (48), we have the following relation between Ω_T and $\Gamma_K(T)$:

$$\Omega_T = -i[\Gamma_K(T) - \Gamma_K(0)]. \quad (49)$$

352 Several expressions have been proposed to describe the temperature-dependence of the Kondo
 353 peak half-width Γ_K in the literature [50–52], which can be used to determine Ω_T . For $T \lesssim T_K$,
 354 an expression beyond Fermi-liquid theory has been derived [52]:

$$\Gamma_K(T) = 1.542T_K \sqrt{(1 + \sqrt{3}) + (2 + \sqrt{3}) \sqrt{1 + \left(\frac{T}{\tilde{T}_K}\right)^2 + \frac{\sqrt{3}}{2} \left(\frac{T}{\tilde{T}_K}\right)^2}}, \quad (50)$$

355 where $\tilde{T}_K \approx 0.491$. Note that Eq. (50) is based on the NRG correction $\Gamma_K(T = 0) \approx 3.7T_K$.
 356 To be consistent with our zero- T treatment, we rescale Eq. (50) by a factor of 3.7. In the
 357 Fermi-liquid regime ($T \ll T_K$), we approximately have

$$\Omega_T = -\frac{\alpha T^2}{T_K}, \quad (51)$$

358 where $\alpha \approx 3.44$. Other ansatz parameters are estimated using the zero- T TDVP approach. The
 359 finite- T spectral function results ($\frac{U}{2t_h} = 2 \times 10^{-3}$, $\Gamma = 0.04U$) are shown in Fig 5. Compared
 360 with NRG results [48], the finite- T Vxc result captures the correct trend of the Kondo peak
 361 width: at $T \ll T_K$, the contribution of Ω_T is negligible, leading to a width dominated by the
 362 Kondo temperature. As T approaches T_K , $|\Omega_T|$ increases. The agreement with NRG results
 363 worsens for $T > 10T_K$. This may be due to our reference expression, Eq. (50), being only
 364 valid for temperatures up to around T_K [52].

365 4 Conclusions and outlook

366 In this work, we applied the exchange-correlation (xc) field formalism to the symmetric single
 367 impurity Anderson model (SIAM) at low temperatures. The formalism introduces a dynamical
 368 xc field (Vxc), which can be interpreted as the Coulomb potential of the xc hole. For the SIAM,
 369 the Vxc also incorporates the hybridization effect between the impurity and the bath. We
 370 proposed an ansatz for the SIAM Vxc, which exhibits different asymptotic behaviors in the

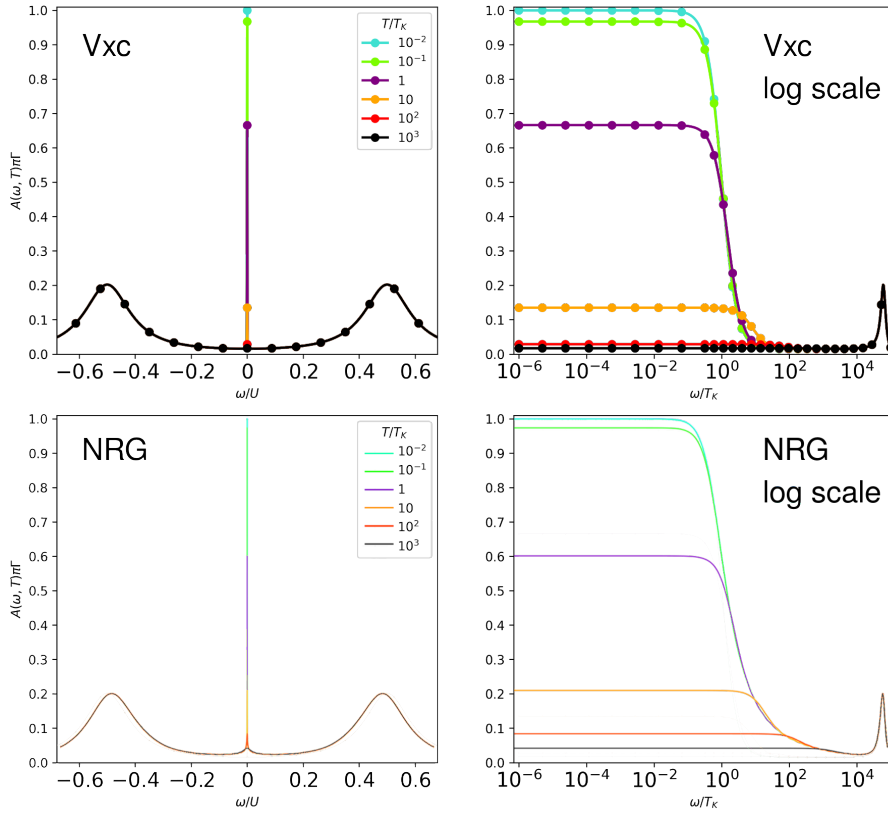


Figure 5: The spectral function of a symmetric SIAM with $\frac{U}{2t_h} = 2 \times 10^{-3}$ and $\Gamma = 0.04U$, at temperatures from $10^{-2}T_K$ to 10^3T_K . Left: The frequency is in unit of U . Right: The frequency is in unit of T_K and in logarithmic scale to highlight the width of the Kondo resonance peak. The NRG results (bottom) are adapted from Ref. [48].

371 small- and large-time regimes, respectively. At small t , the Vxc includes a dominant complex
 372 constant term, \mathcal{C} , and an exponential term with a complex quasiparticle-like excitation, ω_p .
 373 The real and imaginary parts of \mathcal{C} correspond to the peak location and the width of the Hubbard
 374 side-band, respectively. At large t , the Vxc converges to $\mathcal{C} + \omega_p$, which corresponds to the
 375 Kondo peak half-width. Importantly, $\text{Im}[\omega_p(T = 0)]$ accounts for the Kondo temperature. At
 376 zero- T in the WBL, most parameters of the ansatz can be calculated from the model parameters
 377 using Fermi-liquid theory. The only unknown parameter can be estimated by an extrapolation
 378 procedure. For low temperatures, the temperature-dependence of the ansatz parameters is
 379 primarily through $\text{Im}[\omega_p]$, which is determined by extensions of Fermi-liquid theory, guided by
 380 the insights from the auxiliary analytically dimer Vxc. Overall, the spectral function calculated
 381 from the Vxc shows satisfactory agreement with the NRG results. The extrapolation procedures
 382 involved are of low computational cost. We understand the favourable performance of the
 383 xc field formalism as follows: the screening effect underlying the SIAM is essential for the
 384 Kondo effect, and the xc field provides a suitable description for quasiparticle-like excitations.
 385 Hence, the parameters in the ansatz have clear physical meaning and can be related in a
 386 novel perspective to key well-understood features of the spectral function. The fact that only
 387 a few parameters require numerical treatment leads to a good trade-off between accuracy and
 388 computational effort.

389 As an outlook, QIMs beyond the symmetric SIAM at half-filling can also be interpreted
 390 from the perspective of the xc field formalism. We have already noted that for the narrow band

391 SIAM or the SIAM away from half-filling, the V_{xc} requires a different extrapolation scheme.
 392 Additionally, when an external magnetic field is included, the spectral function becomes spin-
 393 dependent, and the Kondo resonance can be suppressed with increasing field. In future work,
 394 we plan to investigate how the magnetic field affects the V_{xc} . Moreover, quantities such as the
 395 dynamical spin susceptibility, the specific heat, and the size of the Kondo cloud are related to
 396 spin correlators. We expect the spin xc field formalism can be applied to these problems.

397 Finally, we stress a significant feature of the xc field formalism: it manages to reduce a
 398 complicated many-body problem to an extrapolation procedure. The extrapolation is usually
 399 done with a (numerically) solvable finite cluster or a homogeneous system as a reference.
 400 When the target system and the reference system exhibit explicit similarities, the extrapolation
 401 can be done straightforwardly. In practice, the connection between the reference system and
 402 the complex target is often less obvious. An example is the SIAM presented in this paper, where
 403 the finite cluster spectral function differs qualitatively from the SIAM. Despite this, the xc field
 404 formalism successfully captures the implicit correspondence, specifically the relative weight
 405 between the Hubbard peak and the Kondo peak at $T = 0$. Hence, we believe that the xc field
 406 formalism, based on the quasiparticle picture, is a viable and powerful approach for modeling
 407 correlated many-body system and holds great potential for first-principles calculations.

408 Acknowledgements

409 I would like to thank Ferdi Aryasetiawan and Claudio Verdozzi for stimulating discussions,
 410 reading the manuscript and providing useful comments.

411 **Funding information** I acknowledge support from the Swedish Research Council (grants
 412 number 2017-03945 and 2022-04486).

413 A Low temperature approximation of the V_{xc}

414 From Eq. (27) and $e^{-\beta E_m} \ll 1$ for $m > 2$, the V_{xc} can be written as

$$V_{p,\sigma}^{xc}(t, \beta) = \frac{C + e^{-\beta \Delta_0} D}{A + e^{-\beta \Delta_0} B}, \quad (\text{A.1})$$

415 where

$$\Delta_0 = E_2 - E_1, \quad (\text{A.2})$$

$$A = \sum_{n_+} a_{n_+,1} e^{-i\omega_{n_+,1} t}, \quad (\text{A.3})$$

$$B = \sum_{n_+} a_{n_+,2} e^{-i\omega_{n_+,2} t}, \quad (\text{A.4})$$

$$C = \sum_{n_+} a_{n_+,1} \omega_{n_+,1} e^{-i\omega_{n_+,1} t}, \quad (\text{A.5})$$

$$D = \sum_{n_+} a_{n_+,2} \omega_{n_+,2} e^{-i\omega_{n_+,2} t}. \quad (\text{A.6})$$

416 An expansion

$$\frac{1}{A + e^{-\beta \Delta_0} B} \approx \frac{1 - e^{-\beta \Delta_0} \frac{B}{A}}{A} \quad (\text{A.7})$$

417 leads to

$$V_{p,\sigma}^{\text{xc}}(t, \beta) = \frac{C}{A} + \left[\frac{D}{A} - \frac{BC}{A^2} \right] e^{-\beta \Delta_0}, \quad (\text{A.8})$$

418 where C/A is just the zero- T Vxc, and all terms of order $\mathcal{O}(e^{-\beta \Delta})$ where $\Delta > \Delta_0$ are neglected
419 for low- T . The time-oscillating term in the main text is then

$$\tilde{V}_{p,\sigma}(t) = \frac{D}{A} - \frac{BC}{A^2} = \frac{C}{A} \left[\frac{D}{C} - \frac{B}{A} \right] \quad (\text{A.9})$$

420 B Analytic Vxc of an impurity-free-electron dimer

421 We use a dimer consisting of an interacting site (f) and a noninteracting site (c) to calculate
422 the analytic Vxc for the f site. Here we repeat the Hamiltonian in the main text:

$$\hat{H}_{\text{dimer}} = \epsilon_f (\hat{n}_{f\uparrow} + \hat{n}_{f\downarrow}) + U \hat{n}_{f\uparrow} \hat{n}_{f\downarrow} + V \sum_{\sigma} (\hat{f}_{\sigma}^{\dagger} \hat{c}_{\sigma} + \text{H.c.}), \quad (\text{B.1})$$

423 where $\epsilon_f = -\frac{U}{2}$, V is the hopping strength and the dimer is at half-filling. With the cho-
424 sen dimer model, the spectral weights and the local Green's function (Eq. (21)) are spin-
425 independent. For simplicity we keep the spin indices implicit in this section. With variables
426 depending on U, V

$$u = \frac{U}{2V} \quad (\text{B.2})$$

$$x = \frac{u}{4} + \sqrt{1 + \left(\frac{u}{4}\right)^2} \quad (\text{B.3})$$

$$y = \frac{u}{2} + \sqrt{1 + \left(\frac{u}{2}\right)^2}, \quad (\text{B.4})$$

427 and the same low- T assumption, the particle part of the Green's function can be written as

$$i\bar{G}_{ff}^P(t) = Z^{-1} \left[a_{1,1} e^{-i\omega_{1,1}t} + a_{2,1} e^{-i\omega_{2,1}t} + e^{\beta u} [a_{1,2} e^{-i\omega_{1,2}t} + a_{2,2} e^{-i\omega_{2,2}t}] \right] \quad (\text{B.5})$$

428 where the partition function is

$$Z = 1 + 3e^{\beta(u-2x)V}, \quad (\text{B.6})$$

429 the spectral weights are

$$a_{1,1} = \frac{(x+y)^2}{2(1+x^2)(1+y^2)} \quad (\text{B.7})$$

$$a_{2,1} = \frac{(1-xy)^2}{2(1+x^2)(1+y^2)} \quad (\text{B.8})$$

$$a_{1,2} = \frac{3}{2(1+y^2)} \quad (\text{B.9})$$

$$a_{2,2} = \frac{3y^2}{2(1+y^2)}, \quad (\text{B.10})$$

430 and the excitation energies are

$$\omega_{1,1} = (2x-y)V \quad (\text{B.11})$$

$$\omega_{2,1} = (2x+y-u)V \quad (\text{B.12})$$

$$\omega_{1,2} = (-y+u)V \quad (\text{B.13})$$

$$\omega_{2,2} = yV. \quad (\text{B.14})$$

431 Following the notations in Appendix A, the zero- T V_{xc} is

$$V_p^{xc}(t, T = 0) = \frac{a_{1,1}\omega_{1,1}e^{-i\omega_{1,1}t} + a_{2,1}\omega_{2,1}e^{-i\omega_{2,1}t}}{a_{1,1}e^{-i\omega_{1,1}t} + a_{2,1}e^{-i\omega_{2,1}t}}. \quad (\text{B.15})$$

432 We note that in the large-interaction regime ($u \gg 1$),

$$x = \frac{u}{2} + \frac{2}{u} + \mathcal{O}\left(\frac{1}{u^3}\right) \quad (\text{B.16})$$

$$y = u + \frac{1}{u} + \mathcal{O}\left(\frac{1}{u^3}\right), \quad (\text{B.17})$$

433 thus

$$\lambda := \frac{a_{1,1}}{a_{2,1}} = \frac{9}{u^2} + \mathcal{O}\left(\frac{1}{u^3}\right) \ll 1. \quad (\text{B.18})$$

434 The expansion of V_{xc} to the first order in λ gives

$$V_p^{xc}(t, T = 0) \approx \omega_{2,1} - \lambda \Omega e^{i\Omega t}, \quad (\text{B.19})$$

435 where

$$\Omega = \omega_{2,1} - \omega_{1,1} = \sqrt{u^2 + 4V}. \quad (\text{B.20})$$

436 For low- T , following Eq. (A.9), we have

$$\frac{\tilde{V}_p(t)}{V_p^{xc}(t, T = 0)} = \frac{a_{1,2}\omega_{1,2}e^{-i\omega_{1,2}t} + a_{2,2}\omega_{2,2}e^{-i\omega_{2,2}t}}{a_{1,1}\omega_{1,1}e^{-i\omega_{1,1}t} + a_{2,1}\omega_{2,1}e^{-i\omega_{2,1}t}} - \frac{a_{1,2}e^{-i\omega_{1,2}t} + a_{2,2}e^{-i\omega_{2,2}t}}{a_{1,1}e^{-i\omega_{1,1}t} + a_{2,1}e^{-i\omega_{2,1}t}}. \quad (\text{B.21})$$

437 Noting that for $u \gg 1$,

$$\frac{a_{1,2}}{a_{2,1}} = \frac{3}{u^2} + \mathcal{O}\left(\frac{1}{u^3}\right), \quad (\text{B.22})$$

$$\frac{a_{2,2}}{a_{2,1}} = 3\left(1 + \frac{4}{u^2}\right) + \mathcal{O}\left(\frac{1}{u^3}\right), \quad (\text{B.23})$$

$$\frac{\omega_{1,1}}{\omega_{2,1}} = \frac{3}{u^2} + \mathcal{O}\left(\frac{1}{u^3}\right), \quad (\text{B.24})$$

$$\frac{\omega_{1,2}}{\omega_{2,1}} = -\frac{1}{u^2} + \mathcal{O}\left(\frac{1}{u^3}\right), \quad (\text{B.25})$$

$$\frac{\omega_{2,2}}{\omega_{2,1}} = 1 - \frac{4}{u^2} + \mathcal{O}\left(\frac{1}{u^3}\right), \quad (\text{B.26})$$

438 we get

$$\frac{\tilde{V}_p(t)}{V_p^{xc}(t, T = 0)} = \frac{24}{u^2}e^{i\Omega't} - \frac{12}{u^2}e^{i\Omega''t} + \mathcal{O}\left(\frac{1}{u^3}\right), \quad (\text{B.27})$$

439 where

$$\Omega' = \omega_{2,1} - \omega_{1,2} = \left(\sqrt{\frac{u^2}{4} + 4} + \sqrt{u^2 + 4} - \frac{u}{2}\right)V \quad (\text{B.28})$$

$$\Omega'' = \omega_{2,1} - \omega_{2,2} = \left(\sqrt{\frac{u^2}{4} + 4} - \frac{u}{2}\right)V. \quad (\text{B.29})$$

440 The temperature factor

$$e^{-\beta\Delta_0} = e^{-\beta(2x-u)} \quad (\text{B.30})$$

441 need to be small in order for the approximation Eq. (A.7) holds.

442 C Calculating the Green's function at $T = 0$ using TDVP

443 Here, we give some details regarding calculating $G_{ff,\sigma}(t, T = 0)$ of our finite cluster using
 444 the ITensor library [43, 44]. We first calculate the ground state $|\Psi_0\rangle$ using the density matrix
 445 renormalization group algorithm. Then the TDVP algorithm is used to time-evolve the state
 446 $\hat{f}_\sigma^\dagger|\Psi_0\rangle$. With $|\Psi(t > 0)\rangle = e^{-i\hat{H}t}\hat{f}_\sigma^\dagger|\Psi_0\rangle$, the one-particle Green's function at equilibrium can
 447 be calculated:

$$\begin{aligned} iG_{ff,\sigma}(t > 0) &= \langle \Psi_0 | e^{i\hat{H}t} \hat{f}_\sigma e^{-i\hat{H}t} \hat{f}_\sigma^\dagger | \Psi_0 \rangle \\ &= e^{iE_0 t} \langle \Psi_0 | \Psi(t) \rangle, \end{aligned} \quad (\text{C.1})$$

448 where E_0 is the ground-state energy. Our system is particle-hole symmetric, which means

$$G_{ff,\sigma}(t < 0, T = 0) = -G_{ff,\sigma}(-t, T = 0). \quad (\text{C.2})$$

449 We calculate the Green's function in the frequency domain with the Fourier transform

$$G_{ff,\sigma}(\omega, T = 0) = \int G_{ff,\sigma}(t, T = 0) e^{i\omega t} dt. \quad (\text{C.3})$$

450 The spectral function is then calculated from $G_{ff,\sigma}(\omega)$.

451 D Solving the Green's function from the ansatz of the Vxc

452 For the SIAM, the equation of motion of the particle Green's function ($t > 0$) reads

$$[i\partial_t - \epsilon_f - V^H - V_{p,\sigma}^{\text{xc}}(t, \beta)] \bar{G}_{ff,\sigma}^p(t, \beta) = 0, \quad (\text{D.1})$$

453 where $\epsilon_f + V^H = 0$ and $g^+ = \bar{G}_{ff,\sigma}^p(t = 0^+, \beta) = -0.5i$ for the symmetric SIAM. Accordingly,
 454 the Green's function is

$$\bar{G}_{ff,\sigma}^p(t > 0, \beta) = g^+ e^{-i \int_0^t V_{p,\sigma}^{\text{xc}}(\bar{t}, \beta) d\bar{t}} \quad (\text{D.2})$$

455 The Vxc is given by the complete ansatz

$$V_{p,\sigma}^{\text{xc}}(t > 0, \beta) = \frac{\lambda(C + \omega_p) + (1 - \lambda)C e^{i\omega_p t}}{\lambda + (1 - \lambda)e^{i\omega_p t}}, \quad (\text{D.3})$$

456 where λ is real and positive, and ω_p and C are complex. Assuming that $\lambda \ll 1$ and $\text{Im}\omega_p > 0$,
 457 we have for positive t

$$V_{p,\sigma}^{\text{xc}}(t, \beta) = \begin{cases} \lambda\omega_p e^{-i\omega_p t} + C, & t \text{ small,} \\ \omega_p + C, & t \text{ large.} \end{cases} \quad (\text{D.4})$$

458 The time integral of V^{xc} is

$$\begin{aligned} \int_0^t V_{p,\sigma}^{\text{xc}}(\bar{t}, \beta) d\bar{t} &= \int_0^t \frac{\lambda(C + \omega_p) e^{-i\omega_p \bar{t}}}{\lambda e^{-i\omega_p \bar{t}} + (1 - \lambda)} d\bar{t} + \int_0^t \frac{(1 - \lambda)C e^{i\omega_p \bar{t}}}{\lambda + (1 - \lambda)e^{i\omega_p \bar{t}}} d\bar{t} \\ &= \frac{C + \omega_p}{-i\omega_p} \ln[\lambda e^{-i\omega_p t} + (1 - \lambda)] + \frac{C}{i\omega_p} \ln[\lambda + (1 - \lambda)e^{i\omega_p t}] \\ &= (C + \omega_p) + i \ln[\lambda + (1 - \lambda)e^{i\omega_p t}]. \end{aligned} \quad (\text{D.5})$$

459 Applying Eq. (D.5) to Eq. (D.2), we obtain the Green's function

$$\bar{G}_{ff,\sigma}^P(t > 0, \beta) = g^+ \left[(1 - \lambda) e^{-iCt} + \lambda e^{-i(C + \omega_p)t} \right]. \quad (\text{D.6})$$

460 The parameters are interpreted as follows: $\text{Im}[C] \sim -\Gamma_H$, where Γ_H is the half-width of the
 461 Hubbard side-band, and $\text{Im}[C + \omega_p] \sim -\Gamma_K$, where Γ_K is the half-width of the Kondo peak and
 462 is much smaller than Γ_H in the Kondo regime. Using the results in the main text, we have
 463 $\lambda \ll 1$, $C + \omega_p = -iT_K$, and $\omega_p = -\frac{U}{2} + i(\Gamma_H - \Gamma_K)$. They are consistent with our assumption
 464 to derive the asymptotic properties in Eq. (D.4).

465 References

- 466 [1] A. C. Hewson, *The Kondo Problem to Heavy Fermions*, Cambridge Studies in Magnetism.
 467 Cambridge University Press (1993).
- 468 [2] Y. Meir, N. S. Wingreen and P. A. Lee, *Low-temperature transport through a quan-*
 469 *tum dot: The anderson model out of equilibrium*, Phys. Rev. Lett. **70**, 2601 (1993),
 470 doi:[10.1103/PhysRevLett.70.2601](https://doi.org/10.1103/PhysRevLett.70.2601).
- 471 [3] D. Goldhaber-Gordon, H. Shtrikman, D. Mahalu, D. Abusch-Magder, U. Meirav and
 472 M. A. Kastner, *Kondo effect in a single-electron transistor*, Nature **391**, 156 (1998),
 473 doi:[10.1038/34373](https://doi.org/10.1038/34373).
- 474 [4] S. M. Cronenwett, T. H. Oosterkamp and L. P. Kouwenhoven, *A Tunable Kondo Effect in*
 475 *Quantum Dots*, Science **281**(5376), 540 (1998), doi:[10.1126/science.281.5376.540](https://doi.org/10.1126/science.281.5376.540),
 476 <https://www.science.org/doi/pdf/10.1126/science.281.5376.540>.
- 477 [5] V. Madhavan, W. Chen, T. Jamneala, M. F. Crommie and N. S. Wingreen, *Tunneling into a*
 478 *Single Magnetic Atom: Spectroscopic Evidence of the Kondo Resonance*, Science **280**(5363),
 479 567 (1998), doi:[10.1126/science.280.5363.567](https://doi.org/10.1126/science.280.5363.567), [https://www.science.org/doi/pdf/10.](https://www.science.org/doi/pdf/10.1126/science.280.5363.567)
 480 [1126/science.280.5363.567](https://www.science.org/doi/pdf/10.1126/science.280.5363.567).
- 481 [6] J. Li, W.-D. Schneider, R. Berndt and B. Delley, *Kondo Scattering Observed at a Single*
 482 *Magnetic Impurity*, Phys. Rev. Lett. **80**, 2893 (1998), doi:[10.1103/PhysRevLett.80.2893](https://doi.org/10.1103/PhysRevLett.80.2893).
- 483 [7] O. Újsághy, J. Kroha, L. Szunyogh and A. Zawadowski, *Theory of the Fano Resonance in*
 484 *the STM Tunneling Density of States due to a Single Kondo Impurity*, Phys. Rev. Lett. **85**,
 485 2557 (2000), doi:[10.1103/PhysRevLett.85.2557](https://doi.org/10.1103/PhysRevLett.85.2557).
- 486 [8] S. Ydman, M. Hopjan and C. Verdozzi, *Nonequilibrium kondo-vs.-rkky scenarios in nan-*
 487 *oclusters*, EPL **123**(4), 47001 (2018), doi:[10.1209/0295-5075/123/47001](https://doi.org/10.1209/0295-5075/123/47001).
- 488 [9] L. Amico, R. Fazio, A. Osterloh and V. Vedral, *Entanglement in many-body systems*, Rev.
 489 Mod. Phys. **80**, 517 (2008), doi:[10.1103/RevModPhys.80.517](https://doi.org/10.1103/RevModPhys.80.517).
- 490 [10] P. Samuelsson and C. Verdozzi, *Two-particle spin entanglement in magnetic anderson nan-*
 491 *oclusters*, Phys. Rev. B **75**, 132405 (2007), doi:[10.1103/PhysRevB.75.132405](https://doi.org/10.1103/PhysRevB.75.132405).
- 492 [11] P. W. Anderson, *Localized Magnetic States in Metals*, Phys. Rev. **124**, 41 (1961),
 493 doi:[10.1103/PhysRev.124.41](https://doi.org/10.1103/PhysRev.124.41).
- 494 [12] A. Georges, G. Kotliar, W. Krauth and M. J. Rozenberg, *Dynamical mean-field theory of*
 495 *strongly correlated fermion systems and the limit of infinite dimensions*, Rev. Mod. Phys. **68**, 13 (1996), doi:[10.1103/RevModPhys.68.13](https://doi.org/10.1103/RevModPhys.68.13).

- 497 [13] S. Biermann, F. Aryasetiawan and A. Georges, *First-Principles Approach to the*
498 *Electronic Structure of Strongly Correlated Systems: Combining the GW Approximation and Dynamical Mean-Field Theory*, Phys. Rev. Lett. **90**, 086402 (2003),
499 doi:[10.1103/PhysRevLett.90.086402](https://doi.org/10.1103/PhysRevLett.90.086402).
500
- 501 [14] G. Kotliar, S. Y. Savrasov, K. Haule, V. S. Oudovenko, O. Parcollet and C. A. Marianetti,
502 *Electronic structure calculations with dynamical mean-field theory*, Rev. Mod. Phys. **78**,
503 865 (2006), doi:[10.1103/RevModPhys.78.865](https://doi.org/10.1103/RevModPhys.78.865).
- 504 [15] H. Aoki, N. Tsuji, M. Eckstein, M. Kollar, T. Oka and P. Werner, *Nonequilibrium*
505 *dynamical mean-field theory and its applications*, Rev. Mod. Phys. **86**, 779 (2014),
506 doi:[10.1103/RevModPhys.86.779](https://doi.org/10.1103/RevModPhys.86.779).
- 507 [16] K. G. Wilson, *The renormalization group: Critical phenomena and the Kondo problem*, Rev.
508 Mod. Phys. **47**, 773 (1975), doi:[10.1103/RevModPhys.47.773](https://doi.org/10.1103/RevModPhys.47.773).
- 509 [17] E. Gull, A. J. Millis, A. I. Lichtenstein, A. N. Rubtsov, M. Troyer and P. Werner, *Continuous-*
510 *time Monte Carlo methods for quantum impurity models*, Rev. Mod. Phys. **83**, 349 (2011),
511 doi:[10.1103/RevModPhys.83.349](https://doi.org/10.1103/RevModPhys.83.349).
- 512 [18] N. Andrei, K. Furuya and J. H. Lowenstein, *Solution of the Kondo problem*, Rev. Mod.
513 Phys. **55**, 331 (1983), doi:[10.1103/RevModPhys.55.331](https://doi.org/10.1103/RevModPhys.55.331).
- 514 [19] P. B. Wiegmann and A. M. Tsvelick, *Exact solution of the Anderson model: I*, J. Phys. C:
515 Solid State Phys. **16**(12), 2281 (1983), doi:[10.1088/0022-3719/16/12/017](https://doi.org/10.1088/0022-3719/16/12/017).
- 516 [20] A. M. Tsvelick and P. B. Wiegmann, *Exact solution of the Anderson model. II. Thermody-*
517 *namic properties at finite temperatures*, J. Phys. C: Solid State Phys. **16**(12), 2321 (1983),
518 doi:[10.1088/0022-3719/16/12/018](https://doi.org/10.1088/0022-3719/16/12/018).
- 519 [21] W. Hofstetter, *Generalized Numerical Renormalization Group for Dynamical Quantities*,
520 Phys. Rev. Lett. **85**, 1508 (2000), doi:[10.1103/PhysRevLett.85.1508](https://doi.org/10.1103/PhysRevLett.85.1508).
- 521 [22] R. Peters, T. Pruschke and F. B. Anders, *Numerical renormalization group approach*
522 *to green's functions for quantum impurity models*, Phys. Rev. B **74**, 245114 (2006),
523 doi:[10.1103/PhysRevB.74.245114](https://doi.org/10.1103/PhysRevB.74.245114).
- 524 [23] A. Weichselbaum and J. von Delft, *Sum-Rule Conserving Spectral Functions from*
525 *the Numerical Renormalization Group*, Phys. Rev. Lett. **99**, 076402 (2007),
526 doi:[10.1103/PhysRevLett.99.076402](https://doi.org/10.1103/PhysRevLett.99.076402).
- 527 [24] Z. Osolin and R. Žitko, *Padé approximant approach for obtaining finite-temperature spec-*
528 *tral functions of quantum impurity models using the numerical renormalization group tech-*
529 *nique*, Phys. Rev. B **87**, 245135 (2013), doi:[10.1103/PhysRevB.87.245135](https://doi.org/10.1103/PhysRevB.87.245135).
- 530 [25] A. Isidori, D. Roosen, L. Bartosch, W. Hofstetter and P. Kopietz, *Spectral function of*
531 *the Anderson impurity model at finite temperatures*, Phys. Rev. B **81**, 235120 (2010),
532 doi:[10.1103/PhysRevB.81.235120](https://doi.org/10.1103/PhysRevB.81.235120).
- 533 [26] A. Ge, N. Ritz, E. Walter, S. Aguirre, J. von Delft and F. B. Kugler, *Real-frequency quantum*
534 *field theory applied to the single-impurity Anderson model*, Phys. Rev. B **109**, 115128
535 (2024), doi:[10.1103/PhysRevB.109.115128](https://doi.org/10.1103/PhysRevB.109.115128).
- 536 [27] D. Zgid, E. Gull and G. K.-L. Chan, *Truncated configuration interaction expansions as*
537 *solvers for correlated quantum impurity models and dynamical mean-field theory*, Phys.
538 Rev. B **86**, 165128 (2012), doi:[10.1103/PhysRevB.86.165128](https://doi.org/10.1103/PhysRevB.86.165128).

- 539 [28] M. Granath and H. U. R. Strand, *Distributional exact diagonalization for-*
540 *malism for quantum impurity models*, Phys. Rev. B **86**, 115111 (2012),
541 doi:[10.1103/PhysRevB.86.115111](https://doi.org/10.1103/PhysRevB.86.115111).
- 542 [29] S. Motahari, R. Requist and D. Jacob, *Kondo physics of the Anderson impurity*
543 *model by distributional exact diagonalization*, Phys. Rev. B **94**, 235133 (2016),
544 doi:[10.1103/PhysRevB.94.235133](https://doi.org/10.1103/PhysRevB.94.235133).
- 545 [30] G. Stefanucci and S. Kurth, *Steady-State Density Functional Theory for Finite Bias Conduc-*
546 *tances*, Nano Letters **15**(12), 8020 (2015), doi:[10.1021/acs.nanolett.5b03294](https://doi.org/10.1021/acs.nanolett.5b03294), PMID:
547 26571349, <https://doi.org/10.1021/acs.nanolett.5b03294>.
- 548 [31] S. Kurth and G. Stefanucci, *Nonequilibrium Anderson model made simple with density*
549 *functional theory*, Phys. Rev. B **94**, 241103 (2016), doi:[10.1103/PhysRevB.94.241103](https://doi.org/10.1103/PhysRevB.94.241103).
- 550 [32] D. Jacob and S. Kurth, *Many-Body Spectral Functions from Steady State Density Functional*
551 *Theory*, Nano Letters **18**(3), 2086 (2018), doi:[10.1021/acs.nanolett.8b00255](https://doi.org/10.1021/acs.nanolett.8b00255), PMID:
552 29437404, <https://doi.org/10.1021/acs.nanolett.8b00255>.
- 553 [33] P. Kubiczek, A. N. Rubtsov and A. I. Lichtenstein, *Exact real-time dynamics of single-*
554 *impurity Anderson model from a single-spin hybridization-expansion*, SciPost Phys. **7**, 016
555 (2019), doi:[10.21468/SciPostPhys.7.2.016](https://doi.org/10.21468/SciPostPhys.7.2.016).
- 556 [34] A. J. Kim, J. Li, M. Eckstein and P. Werner, *Pseudoparticle vertex solver for quantum*
557 *impurity models*, Phys. Rev. B **106**, 085124 (2022), doi:[10.1103/PhysRevB.106.085124](https://doi.org/10.1103/PhysRevB.106.085124).
- 558 [35] D. Werner, J. Lotze and E. Arrigoni, *Configuration interaction based nonequi-*
559 *librium steady state impurity solver*, Phys. Rev. B **107**, 075119 (2023),
560 doi:[10.1103/PhysRevB.107.075119](https://doi.org/10.1103/PhysRevB.107.075119).
- 561 [36] N. Ng, G. Park, A. J. Millis, G. K.-L. Chan and D. R. Reichman, *Real-time evolution of*
562 *Anderson impurity models via tensor network influence functionals*, Phys. Rev. B **107**,
563 125103 (2023), doi:[10.1103/PhysRevB.107.125103](https://doi.org/10.1103/PhysRevB.107.125103).
- 564 [37] B. Kloss, J. Thoenniss, M. Sonner, A. Lerose, M. T. Fishman, E. M. Stoudenmire, O. Par-
565 collet, A. Georges and D. A. Abanin, *Equilibrium quantum impurity problems via ma-*
566 *trix product state encoding of the retarded action*, Phys. Rev. B **108**, 205110 (2023),
567 doi:[10.1103/PhysRevB.108.205110](https://doi.org/10.1103/PhysRevB.108.205110).
- 568 [38] F. Aryasetiawan, *Time-dependent exchange-correlation potential in lieu of self-energy*, Phys.
569 Rev. B **105**, 075106 (2022), doi:[10.1103/PhysRevB.105.075106](https://doi.org/10.1103/PhysRevB.105.075106).
- 570 [39] F. Aryasetiawan and T. Sjöstrand, *Spectral functions of the half-filled one-dimensional*
571 *Hubbard chain within the exchange-correlation potential formalism*, Phys. Rev. B **106**,
572 045123 (2022), doi:[10.1103/PhysRevB.106.045123](https://doi.org/10.1103/PhysRevB.106.045123).
- 573 [40] Z. Zhao, C. Verdozzi and F. Aryasetiawan, *Dynamical exchange-correlation potential for-*
574 *malism for spin- $\frac{1}{2}$ Heisenberg and Hubbard chains: The antiferromagnetic/half-filled case*,
575 Phys. Rev. B **108**, 235132 (2023), doi:[10.1103/PhysRevB.108.235132](https://doi.org/10.1103/PhysRevB.108.235132).
- 576 [41] K. Karlsson and F. Aryasetiawan, *Time-dependent exchange-correlation hole*
577 *and potential of the electron gas*, Phys. Rev. B **107**, 115172 (2023),
578 doi:[10.1103/PhysRevB.107.115172](https://doi.org/10.1103/PhysRevB.107.115172).
- 579 [42] A. L. Fetter and J. D. Walecka, *Quantum Theory of Many-Particle Systems*, Courier Cor-
580 poration (2012).

- 581 [43] M. Fishman, S. R. White and E. M. Stoudenmire, *The ITensor Software Li-*
582 *brary for Tensor Network Calculations*, SciPost Phys. Codebases p. 4 (2022),
583 doi:[10.21468/SciPostPhysCodeb.4](https://doi.org/10.21468/SciPostPhysCodeb.4).
- 584 [44] M. Fishman, S. R. White and E. M. Stoudenmire, *Codebase release 0.3 for ITensor*, SciPost
585 Phys. Codebases pp. 4–r0.3 (2022), doi:[10.21468/SciPostPhysCodeb.4-r0.3](https://doi.org/10.21468/SciPostPhysCodeb.4-r0.3).
- 586 [45] J. Haegeman, J. I. Cirac, T. J. Osborne, I. Pižorn, H. Verschelde and F. Verstraete, *Time-*
587 *Dependent Variational Principle for Quantum Lattices*, Phys. Rev. Lett. **107**, 070601
588 (2011), doi:[10.1103/PhysRevLett.107.070601](https://doi.org/10.1103/PhysRevLett.107.070601).
- 589 [46] M. Yang and S. R. White, *Time-dependent variational principle with ancillary Krylov sub-*
590 *space*, Phys. Rev. B **102**, 094315 (2020), doi:[10.1103/PhysRevB.102.094315](https://doi.org/10.1103/PhysRevB.102.094315).
- 591 [47] P. Nozières, *A “fermi-liquid” description of the Kondo problem at low temperatures*, J. Low
592 Temp. Phys. **17** (1974), doi:[10.1007/BF00654541](https://doi.org/10.1007/BF00654541).
- 593 [48] E. Pavarini, E. Koch, A. Lichtenstein and D. Vollhardt, eds., *Dynamical Mean-Field Theory*
594 *of Correlated Electrons: Modeling and Simulation*, Verlag des Forschungszentrum Jülich,
595 ISBN ISBN 978-3-95806-619-9 (2022).
- 596 [49] R. Žitko and T. Pruschke, *Energy resolution and discretization artifacts in*
597 *the numerical renormalization group*, Phys. Rev. B **79**, 085106 (2009),
598 doi:[10.1103/PhysRevB.79.085106](https://doi.org/10.1103/PhysRevB.79.085106).
- 599 [50] H. O. Frota, *Shape of the kondo resonance*, Phys. Rev. B **45**, 1096 (1992),
600 doi:[10.1103/PhysRevB.45.1096](https://doi.org/10.1103/PhysRevB.45.1096).
- 601 [51] K. Nagaoka, T. Jamneala, M. Grobis and M. F. Crommie, *Temperature De-*
602 *pendence of a Single Kondo Impurity*, Phys. Rev. Lett. **88**, 077205 (2002),
603 doi:[10.1103/PhysRevLett.88.077205](https://doi.org/10.1103/PhysRevLett.88.077205).
- 604 [52] D. Jacob, *Temperature evolution of the Kondo peak beyond Fermi liquid theory*, Phys. Rev.
605 B **108**, L161109 (2023), doi:[10.1103/PhysRevB.108.L161109](https://doi.org/10.1103/PhysRevB.108.L161109).